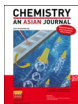


VIP Design and Fabrication of Tubular Micro/Nanomotors via 3D Laser
LithographySPECIAL
ISSUE Yimeng Chen, Borui Xu, and Yongfeng Mei*^[a]

Abstract: Catalytic tubular micro/nanomachines convert chemical energy from a surrounding aqueous fuel solution into mechanical energy to generate autonomous movements, propelled by the oxygen bubbles decomposed by hydrogen peroxide and expelled from the microtubular cavity. With the development of nanotechnology, micro/nanomotors have attracted more and more interest due to their numerous potential for in vivo and in vitro applications. Here, highly efficient chemical catalytic microtubular motors were fabricated via 3D laser lithography and their motion

behavior under the action of driving force in fluids was demonstrated. The frequency of catalytically-generated bubbles ejection was influenced by the geometrical shape of the micro/nanomotor and surrounding chemical fuel environment, resulting in the variation in motion speed. The micro/nanomotors generated with a rocket-like shape displayed a more active motion compared with that of a single tubular micro/nanomotor, providing a wider range of practical micro-/nanoscale applications in the future.

Introduction

In recent years, nanotechnology is an emerging science and highly concerned subject. Micro/nanomotors are nano- and microscale functional devices with self-propelled characteristics.^[1–3] They can convert all kinds of energy in the environment into mechanical energy to generate autonomous movement,^[4,5] which can be used to pick up, transport and release various micro/nanoscale objects in liquid medium. Therefore, micro/nanomotor has a variety of important potential applications in the fields ranging from drug delivery to pollution delamination, causing more and more interest.^[6–8] Due to the simple structure of micro/nanomotor and the controllability of its direction and speed, remarkable progress has been made in many orientations such as motion control and functionalization of micro/nanomotors.^[9–12] With advanced microfabrication methods, micro/nanomotors have been designed into distinct geometries to transfer the forces for their autonomous movement with high efficiency including tubes,^[1,12–16] Janus spheres,^[17] rods,^[2,18] helices^[19,20] and other structural forms of micro/nanomotors.^[21,22] Among all kinds of micro/nanomotors, tubular micro/nanomotors have stimulated a lot of interest due to its good performance in terms of speed and direction control. Therefore, so far, there has been much effort towards

exploring the mechanism of motion and developing potential applications of tubular micro/nanomotors.^[11,23–25] The motion of these tubular micro/nanomotors is normally achieved through the chemical propulsion mechanism, which mainly relies on the participation of chemical fuels such as hydrogen peroxide and corresponding catalyst in the medium environment to convert chemical energy into mechanical energy. The most common chemical reaction used in catalytic self-propulsion is the decomposition of H₂O₂ under the action of metallic layer such as Pt or Ag.^[1,3,8,9,17,26–32] The locomotion including the motion speed and state of tubular micro/nanomotors, can be adjusted by the factors as geometrical shape of micro/nanomotors, concentration of external chemical fuel environment and magnetic field intensity.^[33–36]

Variety of methods were utilized to increase the speed of self-propelled micro/nanomotors which can execute more complex tasks such as protein separation, drug delivery, environment detection and repair.^[21,37–40] Recently, various approaches were employed to fabricate catalytic tubular micro/nanomotors, among which the most common methods are rolled-up nanotechnology technique and template-assisted electrochemical deposition.^[1,14,31,41–44] To construct asymmetric tubular micro/nanostructures, another advanced technique is 3D printing technology, which is a new rapid prototyping technique and has received extensive attention worldwide.^[45] 3D laser lithography was developed to address a series of micro- and nanoscale materials. Two-photon polymerization lithography is a common method applied in 3D direct laser writing (3D-DLW) technology which is mainly utilized in this experiment.^[46,47] 3D-DLW has been proved to be a versatile tool for manufacturing complex and high-quality structures with nanometer precision and accuracy in three dimensional space. This technique makes it possible to demonstrate some complicated micro/nanostructures that are difficult to achieve using traditional preparation methods, and the advantages are particular-

[a] Y. Chen, B. Xu, Prof. Y. Mei
Department of Materials Science
State Key Laboratory of ASIC and Systems
Fudan University
Shanghai 200433 (China)
E-mail: yfm@fudan.edu.cn

Supporting information and the ORCID identification number(s) for the author(s) of this article can be found under:
<https://doi.org/10.1002/asia.201900300>.

SPECIAL
ISSUE This manuscript is part of a special issue on Smart Chemistry, Smart Motors. Click here to see the Table of Contents of the special issue.

ly evident in consideration of the construction of some challenging three-dimensional structures in micro and nano-scale.^[22,48,49]

In this article, we present an innovative method for fabricating micro/nanomotors via employing 3D-DLW lithography in a negative photoresist to pattern shapes into tubular structures. The fabricated microtube evaporated with metallic layer as catalyst can produce movements in hydrogen peroxide solution. The geometric parameters and aqueous H₂O₂ solution concentration were investigated on the microtubular cavity fixed on the substrate to uncover their influence on the oxygen bubble ejection frequency. It turns out that the bubble expelling frequency increases with the cavity length and chemical fuel concentration, which reflects on the hydrodynamic performance of micro/nanomotor. Furthermore, we demonstrated the catalytic motion activity of tubular micro/nanomotor prepared by 3D-DLW lithography in hydrogen peroxide solution, and proposed an advanced rocket-shape microstructure design, performing an enhancement on speed which provides new possibilities for better applications.

Experimental Section

The tubular micro/nanomotors were prepared via 3D-DLW lithography. To fabricate such a micro/nanomotor, the geometries of microtube should be designed first. The structures to be fabricated on the glass substrate were modeled using Describe software (see Figure S1 in supporting information). The standard lithography file which describes stepwise bottom-up path traces and laser power information, can be translated into command for 3D laser lithography equipment (Nanoscribe GmbH). Coordinates and laser intensities to be polymerized via photon absorption are contained in the GWL file. In the process of 3D lithography, DLW employs a femtosecond-pulsed laser operating at wavelength of 780 nm to cross-link the photoresist into a designed structure which is based on a two-photon polymerization technique.

Figure 1 details the fabrication process of the catalytic tubular micro/nanomotors in this experiment. As shown in Figure 1 a, the objective was dipped into a liquid negative-tone photoresist drop hanging at a glass substrate which was placed on a holder that fits the piezoelectric x–y–z stage. The photoresist IP-Dip was used as the base material for the fabricated sample of which the refractive

index is matched to the objective. The galvo scanner determines the laser trajectories in the exposed photoresist volume through scanning the focal point of a femtosecond laser. Then the microstructures were removed from the sample holder and developed in polyethylene glycol methacrylate (PEGMA) for 30 minutes, followed by a rinsing step in isopropyl alcohol (IPA) before drying in a critical point dryer (CPD). After development and removing of photoresist with solvent, the sample containing an array of microtubes was obtained on the glass substrate (Figure 1 b).

In order to realize the chemical reaction of hydrogen peroxide decomposition into oxygen and H₂O, noble metal layer (such as Pt) was placed inside the microtube. After the step of structure printing, Pt layer with thickness of 4 nm was deposited onto the inner wall of microtube by e-beam evaporation, which was used as a catalyst to decompose H₂O₂ (Figure 1 c). In the following experimental procedures, for the micro/nanomotors on chip, we directly drop tiny aqueous H₂O₂ solution on the glass substrate and observe the oxygen bubble generation and ejection from the end part of the tubular micro/nanomotor. To observe their self-propelled movement in hydrogen peroxide, the microstructures were removed from the glass substrate by a micromanipulator equipped with a syringe needle to release them into H₂O₂ solution (Figure 1 d). Then they were propelled by catalytically-produced O₂ gas bubbles in aqueous solution which was observed under optical microscope and recorded by CCD camera (Figure 1 e).

Results and Discussion

Structure of tubular micro/nanomotor

After completion of two-photon polymerization lithography, samples were imaged via optical microscopy (optical microscope images were seen in Figure S2 in the supporting information) and field-emission scanning electron microscopy (FE-SEM). Successful fabrication of an array of microtubular structure in Figure 2a proves its ability in high-yield fabrication. SEM images of micro/nanomotors show successful fabrication of programmable and controllable geometry of the structure at the micro-/nanoscale. For the convenience of e-beam evaporation, the geometry of micro/nanomotor was specially designed to be conical tubular microstructures with larger upper base and smaller bottom base, as displayed in Figure 2b. The process resolution limitation from the combination of laser lithography system and photoresist used in the fabrication pro-

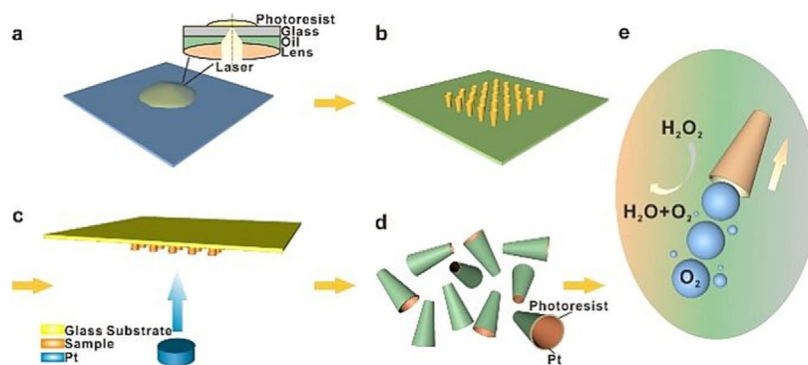


Figure 1. Schematic diagrams of fabrication of tubular micro/nanomotors a) The principle of direct laser writing. b) Fabricated samples using 3D-DLW lithography technology. c) Deposition of Pt layer onto the inner wall of the cavity by e-beam evaporation. d) Release of micro/nanomotors with Pt inner wall. e) The tubular micro/nanomotors was propelled by expelled O₂ gas bubbles.

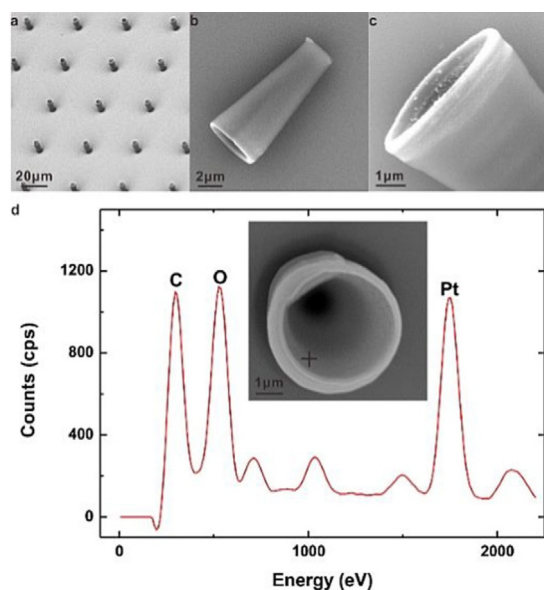


Figure 2. Characterization of microtubular structure. a) SEM image of an array of microtubes on glass substrate fabricated by 3D-DLW lithography b) SEM image of the structure of obtained tubular micro/nanomotor. c) SEM image of the cross view of the tubular cavity with Pt nanoparticles inside. d) Spectrum of the elemental analysis of one spot on the inner wall of microtube.

cess led to the discrepancies between the fabricated structure and designed model. In 3D-DLW lithography, the asymmetric fabrication method was applied to prepare our micro/nanomotors in which ultrashort laser beam focus is scanned circle-by-circle and layer-by-layer. The radius of circular routes increases gradually in each layer by a certain proportion until the designed height is obtained. To make the catalyst prepared inside the microtube, Pt layer was deposited onto the inner surface of tubular cavity by e-beam evaporation. Figure 2c shows a SEM image of the cross view of a microtube. It is observed that some particles were grown on the inner wall, proving that metallic catalyst Pt was inside the microtubular structure, which was further confirmed by elemental analysis of the inner wall as indicated in Figure 2d.

Bubble ejection from micro/nanomotor

In order to observe the evolution of generated oxygen bubble, we firstly defined the geometric parameters of tubular micro/nanomotor on the chip as shown in Figure 3a. The microtube is a conical tube in shape with length L with two openings, whose radii are defined as R_1 and R_2 , and semi-cone angle θ . The diameter of the larger opening of the microtube is c.a. $10\ \mu\text{m}$ ($R_2 = 5\ \mu\text{m}$) and the diameter of the smaller opening is c.a. $5\ \mu\text{m}$ ($R_1 = 2.5\ \mu\text{m}$). The thickness of the tube wall is estimated to be c.a. $0.5\ \mu\text{m}$. The values of R_1 and R_2 were fixed to explore the relationship between bubble generation frequency and micro/nanomotor length, which reflects the motion behavior of fabricated tubular micro/nanomotors related to the geometry. The Figure 3b presents a fabricated microtube with above geometric parameters.

When the catalytic micro/nanomotor was immersed into aqueous H_2O_2 solution, produced O_2 gas bubbles were ejected from one tube end (Figure 3c). The video of the bubble ejection from the microtube can be seen in Video S1 in the supporting information. The conical tubular shape of micro/nanomotor restricts the bubble to expand in one direction. The decomposition of hydrogen peroxide produced a high concentration of oxygen on the catalyst surface, and the oxygen accumulating at the surface forms bubble in a critical nucleation radius. Dissolved oxygen continues to spread to bubbles causing them to grow up under the effect of dissolved gas diffusion, and then release from the surface as the bubble grows to a separate radius.^[26,28,50] Previous experimental results indicated that when the fluid is sucked in from the smaller opening, the bubbles migrate mainly towards larger tubular opening.^[29,50] The force acts on the tubular cavity and bubble during the bubble growth at one end of the microtube. When the bubble exits the cone, one bubble cycle is finished. The oxygen bubble ejection frequency can affect the average velocity of a micro/nanomotor. To characterize the influence of the geometric parameters of micro/nanomotor on bubble ejection frequency, bubble ejection period ΔT was recorded, generated from micro/nanomotors with different lengths L on chip surrounding by 2% concentration of H_2O_2 , and the ejection fre-

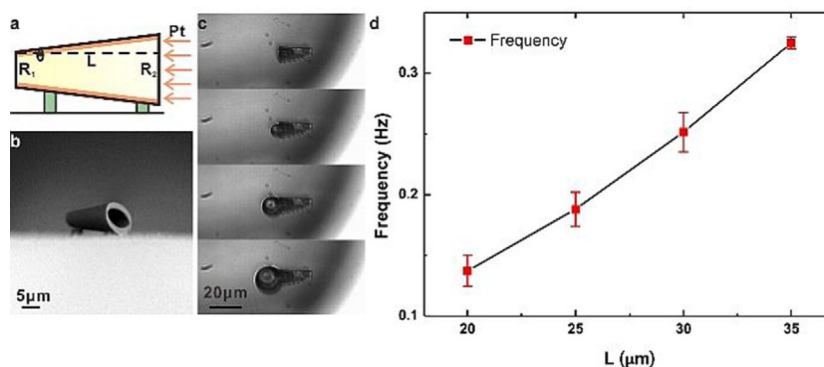


Figure 3. a) Schematic diagram of designed tubular micro/nanomotor on chip. b) SEM image of fabricated tubular microstructure on chip. c) Time-lapse images of the bubble ejection from tubular micro/nanomotor ($L = 20\ \mu\text{m}$) in 2% concentration of H_2O_2 . d) Average bubble ejection frequency ($1/\Delta T$) of micro/nanomotors related to the tubular cavity length in 2% concentration of H_2O_2 .

quency is defined as $1/\Delta T$. As shown in Figure 3d, the frequency of bubble ejection from the end of conical tube increases with the length of micro/nanomotor, which leads to the conclusion that bubble expelling frequency of the micro/nanomotor with a larger length is higher than that of a smaller one.

In addition, the role of chemical fuel concentration was investigated on a micro/nanomotor with length of 25 μm to study the relationship between bubble ejection frequency and concentration. Figure 4 shows the average bubble ejection frequency

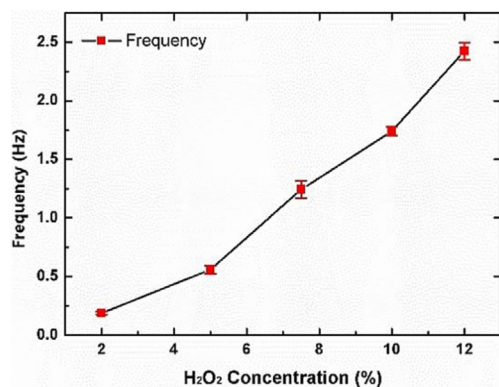


Figure 4. The average bubble ejection frequency ($1/\Delta T$) of micro/nanomotor ($L = 25 \mu\text{m}$) in the presence of H_2O_2 fuel solution with different concentrations.

quency $1/\Delta T$ as a function of hydrogen peroxide concentration (including 2%, 5%, 7.5%, 10% and 12%). It is noted that the frequency of bubble ejection from the micro/nanomotor increases with the rising of H_2O_2 fuel concentration as a result of the acceleration of chemical catalytic reaction ($\text{H}_2\text{O}_2 \rightarrow \text{H}_2\text{O} + \text{O}_2$). When the concentration of hydrogen peroxide solution is further risen, bubble ejection frequency of tubular micro/nanomotors becomes significantly faster in higher H_2O_2 fuel concentration solutions and tended to be stable in further higher H_2O_2 fuel concentration solutions due to the saturation of catalytic reaction (Figure S3).

Motion behavior of fabricated tubular micro/nanomotors

Figure 5 illustrates the locomotion behavior of fabricated micro/nanomotors with identical diameter (10 μm and 5 μm) and length (15 μm) in 5% H_2O_2 solution.

The position of micro/nanomotors in every 200 ms is shown in Figure 5a and its trajectory is highlighted in Figure 5b (see the Video S2 in the supporting information). When the catalytic micro/nanomotor was positioned into the chemical fuel H_2O_2 , produced O_2 gas bubbles were ejected from one tube end and thrust the microtube. The recoiling propulsion mechanism of oxygen bubbles of tubular micro/nanomotor is closely related to the decomposition of hydrogen peroxide.^[26,28] Produced oxygen coalesced into bubbles, and then diffused to a bubble nucleation center at one end of the micro/nanomotor. When the oxygen bubble grew up and departed from one end of the microtube cavity, this separation led to a change in momentum. According to the principle of momentum conserva-

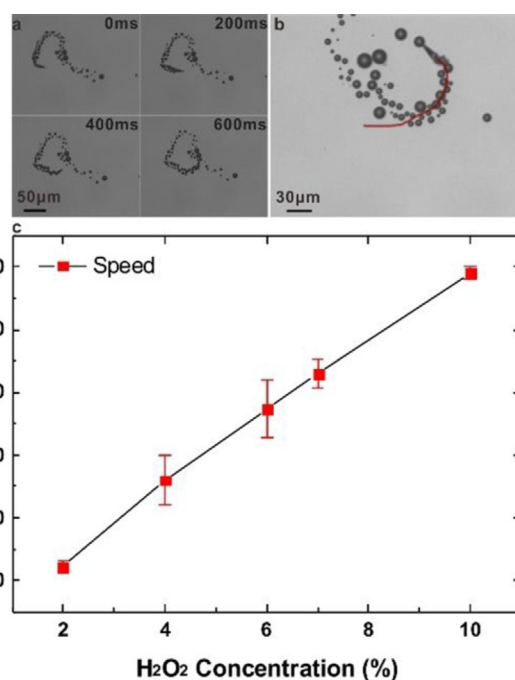


Figure 5. a) Time-lapse images of the motion of a tubular micro/nanomotor in 5% H_2O_2 solution. b) A typical motion trajectory of the tubular micro/nanomotor in 5% H_2O_2 solution. c) The average speed of fabricated tubular micro/nanomotor with the length of 12 μm in the presence of H_2O_2 fuel solution in different concentrations.

tion, the bubble will produce a counter-thrust to drive the motion of the micro/nanomotor. Because in the chemical reaction, the catalyst will not be consumed, as long as the hydrogen peroxide exists, the new bubbles will be generated and released continuously, which leads to the continuous propulsion movement of micro/nanomotor in aqueous H_2O_2 fuel solution. The micro/nanomotor moved in circular path for the reason of the asymmetry in its microtubular structure, causing the force perpendicular to the axis of the microtube unbalanced. To further control the direction of motion, the micro/nanomotor could be coated with metallic Fe layer inside gave an response to the external magnetic field.^[5,11] Moreover, the dependence of the micro/nanomotor velocity on the chemical fuel concentration was investigated as shown in Figure 5c. In 2% concentration H_2O_2 aqueous solution, the tubular micro/nanomotor moved in $24.3 \mu\text{m s}^{-1}$ and had an increase to $75 \mu\text{m s}^{-1}$ in 6% concentration H_2O_2 aqueous solution. The average speed of the micro/nanomotor could reach the $118 \mu\text{m s}^{-1}$ in 10% concentration H_2O_2 aqueous solution and the maximum velocity could be attained at $120.5 \mu\text{m s}^{-1}$. As the concentration of H_2O_2 increases, the micro/nanomotor moves faster.

Comparison between motions of micro/nanomotors

In daily life, it is noticed that man-made rocket consists of a giant core stage flanked by four solid rocket boosters to accelerate the flight of the rocket. Figure 6a shows a sketch of counterparts of the rocket in which boosters are located at the rear part. This enlightens us to design a similar structure of

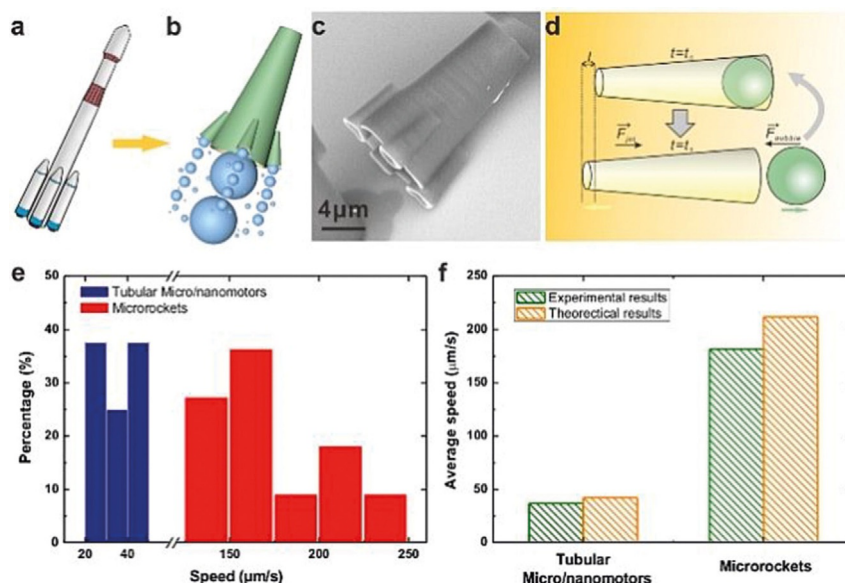


Figure 6. a) Model of a rocket in the macro world b) Schematic diagram of a tubular microrocket c) SEM images of tubular micro/nanomotors with a similar structure like the rocket boosters which is inspired by the macro rocket. d) Schematic diagram of the micro/nanomotor bubble circulation process from the bubble forming inside to the bubble departing from the microtube. e) Comparison of average motion velocities between two kinds of different micro/nanomotors. f) The average speed of tubular micro/nanomotors and microrockets in theoretical results and experimental results for comparison.

micro/nanomotor with some attachments to improve the motion speed in the solution. The schematic diagram of our designed structure is displayed in Figure 6b. And corresponding micro/nanomotor after the deposition of metallic layer was demonstrated in Figure 6c, which proves that this designed structure is available with 3D-DLW lithography. The diameter of the larger opening of the mainbody is c.a. 10 μm and the diameter of the smaller one is c.a. 5 μm. The length of the mainbody is c.a. 15 μm. Four rocket-booster-like counterparts was about a quarter size of the mainbody and located at the rear part, which constituted a new kind of micro/nanomotor similar with a microrocket. With regard to the microrocket, it is expected that the rocket-like micro/nanomotors can attain more reverse thrust to push its motion in the possession of booster parts. Corresponding recoiling force caused by the growth of produced oxygen bubble is the propulsion force to move the micro/nanomotor forward in the opposite direction.

As aforementioned, it is illustrated that the bubble ejection from the tubular cavity propels the catalytic micro/nanomotor step by step and each bubble pushes the micro/nanomotor forward by one step length (Figure 6d). Previous study inferred that the average micro/nanomotor velocity quantitatively depends upon the bubble expelling frequency and the corresponding moving step length, which can be determined by the generation rate and size of produced oxygen bubbles.^[26]

For a conical tubular micro/nanomotor with two openings radii R_1 and R_2 , a length of L and a semi-cone θ , the oxygen bubble productivity can be expressed as^[28]

$$k = dVO_2/dt = nCH_2O_2S = nCH_2O_2\pi L(2R_2 - L \tan \theta) / \cos \theta$$

Where n is a rate constant experimentally estimated to be $9.8 \times 10^{-4} \text{ ms}^{-1}$ from both flat and rolled surfaces in H_2O_2 with

concentrations up to $\approx 10\%$.^[26] The bubble expelling frequency can be deduced as following:

$$f = nCH_2O_2S / V_{bubble} = \frac{nCH_2O_2\pi L(2R_2 - L \tan \theta) / \cos \theta}{4\pi R_b^3 / 3} = \frac{3nCH_2O_2L(2R_2 - L \tan \theta)}{4R_b^3 \cos \theta}$$

\vec{F}_{bubble} and \vec{F}_{jet} are the drag forces acting on the bubble and micro/nanomotor, respectively. Stoke's law can be utilized to estimate the value of \vec{F}_{bubble} which is expressed as^[26]

$$\vec{F}_{bubble} = -6\pi\mu R_b \vec{v}_b(t)$$

Where R_b is the bubble radius and μ is the fluid viscosity. \vec{F}_{jet} is parallel to the center line of the microtube which can be approximately expressed as^[26]

$$\vec{F}_{jet} = -\frac{2\pi\mu L \vec{v}_j(t)}{\ln\left(\frac{2L}{2R_2 - L \tan \theta}\right) + const}$$

where L is the length, R_2 is the maximum radius of the micro/nanomotor, θ is the semi-cone angle of the conical tube and $const$ is a constant value determined by the geometry of the micro/nanomotor. As presented by Li, et al.,^[26] the equation using the conservation of momentum can be expressed as

$$\int_{t_0}^{t_1} \vec{F}_{bubble} dt + \int_{t_0}^{t_1} \vec{F}_{jet} dt = 0$$

where t_0 is the initial time and t_1 is the final time. Therefore,

$$\int_{t_0}^{t_1} \vec{v}_j(t) dt + \int_{t_0}^{t_1} \vec{v}_b(t) dt = 2Rb$$

where $\vec{v}_j(t)$ and $\vec{v}_b(t)$ are the velocities of the micro/nanomotor and the bubble.

Combing previous equations, we can get the displacement of the micro/nanomotor in one step written as

$$l = \frac{6Rb^2}{3Rb + L / (\ln(\frac{2L}{2R_2 - L \tan \theta}) + \text{const})}$$

Thus, the average velocity of the conical tubular micro/nanomotor can be expressed as

$$v_j = f \times l = \frac{9nCH_2O_2L(R_2 - L/2 \tan \theta)}{3Rb^2 \cos \theta + LRb \cos \theta / (\ln(\frac{2L}{2R_2 - L \tan \theta}) + \text{const})}$$

Where f is the bubble expelling frequency. The equation above indicates that f bubbles are ejected from the end of the micro/nanomotor in one second, and correspondingly propel the micro/nanomotor f steps forward.

For the microrocket with four rocket-booster-like structures which are about a quarter size of the main microtube cavity, $R_c = 1/4R_2$, $L_c = 1/4 L$, $R_{bc} = 1/4R_b$, in which R_c is the maximum radius, L_c is the length of the smaller micro/nanomotor, and R_{bc} is the radius of the bubbles from the rocket-booster-like counterpart. Thus the frequency of bubble ejection and displacement of micro/nanomotor in one step can be expressed as

$$f_c = \frac{3nCH_2O_2L_c(2R_c - L_c \tan \theta)}{4R_{bc}^3 \cos \theta} = \frac{3nCH_2O_2L(2R_2 - L \tan \theta)}{Rb^3 \cos \theta} = 4f$$

$$l_c = \frac{3Rb^2}{6Rb + 2L / (\ln(\frac{2L}{2R_2 - L \tan \theta}) + \text{const})} = 1/4l$$

And

$$v_c = 4f \times 1/4l = v_j$$

which shows that $4f$ bubbles are ejected from the end of the smaller microtube in one second, and correspondingly propel the smaller microtube $4f$ steps forward.

From the above, the microrocket can provide more openings to draw in the H_2O_2 chemical fuel, causing more production of oxygen bubbles, and this suggests that more bubbles are ejected from the microrocket in the same period than from an ordinary tubular micro/nanomotor. Therefore, it is roughly estimated that the average microrocket velocity is about 5 times larger than tubular micro/nanomotor, $v_r \approx 5v_j$. The theoretical results are compared with our experimental results.

The movement of conventional tubular micro/nanomotors without advanced structure design and micro/nanomotors with rocket-booster-like structures are studied for comparison. To further understand the catalytic motion behavior of the micro/nanomotors, the statistics of the motion speed were collected according to the experimental observation of several

micro/nanomotors moving in the aqueous H_2O_2 solution. The histograms of the velocity distribution of the motion in 3% aqueous H_2O_2 solution of selected micro/nanomotors are displayed in Figure 6e, in which the vertical coordinate of this bar chart represents the percentage of micro/nanomotors in a certain speed range. In 3% concentration H_2O_2 fuel solution, the average speed of microrockets increased to $181.7 \mu m s^{-1}$ compared with $36.8 \mu m s^{-1}$ in the case of tubular micro/nanomotors. The maximum of speed at $250 \mu m s^{-1}$ was achieved by microrockets. As plotted in Figure 6f, compared with the ordinary tubular micro/nanomotors, microrockets made a nearly fivefold enhancement in motion speed, which matches well with theoretical calculation.

Conclusions

In summary, we prepared a micro/nanomotor with a tubular structure through a kind of different manufacturing technique named as 3D direct laser writing lithography, which is a rising rapid prototyping technology in recent years. The advantage of this fabrication method is that it is possible to design the structure of micro/nanomotor according to our demand in practical applications. Then, the dependence of bubble ejection frequency on the micro/nanomotor geometries and external chemical environment factors was explored. The bubble expelling frequency of the micro/nanomotor increases with increasing length of the microtube and concentration of chemical fuel H_2O_2 . We also found that the moving speed of the micro/nanomotor improves with an increase of the concentration of hydrogen peroxide solution. Furthermore, another kind of tubular micro/nanomotor with a structure like rocket boosters was designed to accelerate the motion. Compared with ordinary tubular micro/nanomotors, the microrockets have much higher average speed, which is well explained with theoretical analysis. As experimentally proved by tracking the motion of self-propelled micromachines via chemical reaction in H_2O_2 solution using microscopy, their highly efficient propulsion via the catalytic decomposition of hydrogen peroxide fuel results in an enhancement in the speed of microrockets. Because high concentrations of hydrogen peroxide are harmful to biological materials and tissues, for biomedical transports and processes, chemically propelled high-speed micro/nanomotors in fuel solutions of low concentration are more advantageous. Therefore, these tubular micro/nanomotors are able to effectively carry out many complex demanding tasks and have a wide range of potential micro- and nanoscale applications.

Acknowledgements

This work is supported by the Natural Science Foundation of China (51322201, U1632115), Science and Technology Commission of Shanghai Municipality (17JC1401700), the National Key Technologies R&D Program of China (2015ZX02102-003) and the Changjiang Young Scholars Program of China. Part of the experimental work has been carried out in Fudan Nanofabrication Laboratory.

Conflict of interest

The authors declare no conflict of interest.

Keywords: 3D lithography · autocatalysis · chemical propulsion · nanotechnology · tubular micro/nanomotor

- [1] Y. F. Mei, A. A. Solovev, S. Sanchez, O. G. Schmidt, *Chem. Soc. Rev.* **2011**, *40*, 2109–2119.
- [2] J. Wang, *ACS Nano* **2009**, *3*, 4–9.
- [3] G. A. Ozin, I. Manners, S. Fournier-Bidoz, A. Arsenault, *Adv. Mater.* **2005**, *17*, 3011–3018.
- [4] F. J. Zha, T. W. Wang, M. Luo, J. G. Guan, *Micromachines* **2018**, *9*, 78.
- [5] M. Zarei, M. Zarei, *Small* **2018**, *14*, 1800912.
- [6] J. Wang, W. Gao, *ACS Nano* **2012**, *6*, 5745–5751.
- [7] W. Wang, W. Duan, S. Ahmed, T. E. Mallouk, A. Sen, *Nano Today* **2013**, *8*, 531–554.
- [8] G. J. Zhao, N. T. Nguyen, M. Pumera, *Nanoscale* **2013**, *5*, 7277–7283.
- [9] B. R. Xu, B. R. Zhang, L. Wang, G. S. Huang, Y. F. Mei, *Adv. Funct. Mater.* **2018**, *28*, 1705872.
- [10] D. Kagan, R. Laocharoensuk, M. Zimmerman, C. Clawson, S. Balasubramanian, D. Kang, D. Bishop, S. Sattayasamitsathit, L. Zhang, J. Wang, *Small* **2010**, *6*, 2741–2747.
- [11] A. A. Solovev, S. Sanchez, M. Pumera, Y. F. Mei, O. G. Schmidt, *Adv. Funct. Mater.* **2010**, *20*, 2430–2435.
- [12] G. S. Huang, J. Wang, Y. F. Mei, *J. Mater. Chem.* **2012**, *22*, 6519–6525.
- [13] A. A. Solovev, Y. F. Mei, E. Bermúdez Urena, G. S. Huang, O. G. Schmidt, *Small* **2009**, *5*, 1688–1692.
- [14] W. Gao, S. Sattayasamitsathit, J. Orozco, J. Wang, *J. Am. Chem. Soc.* **2011**, *133*, 11862–11164.
- [15] K. M. Manesh, M. Cardona, R. Yuan, M. Clark, D. Kagan, S. Balasubramanian, J. Wang, *ACS Nano* **2010**, *4*, 1799–1804.
- [16] Y. F. Mei, G. S. Huang, A. A. Solovev, E. Bermudez Urena, I. Monch, F. Ding, T. Reindl, R. K. Y. Fu, P. K. Chu, O. G. Schmidt, *Adv. Mater.* **2008**, *20*, 4085–4090.
- [17] J. G. Gibbs, Y.-P. Zhao, *Appl. Phys. Lett.* **2009**, *94*, 163104.
- [18] D. Kagan, P. Calvo-Marzal, S. Balasubramanian, S. Sattayasamitsathit, K. M. Manesh, G. Flechsig, J. Wang, *J. Am. Chem. Soc.* **2009**, *131*, 12082–12083.
- [19] A. Ghosh, P. Fischer, *Nano Lett.* **2009**, *9*, 2243–2245.
- [20] S. Schuerle, S. Pané, E. Pellicer, J. Sort, M. D. Baro, B. J. Nelson, *Small* **2012**, *8*, 1498–1502.
- [21] J. X. Li, B. E. Fernandez de Avila, W. Gao, L. F. Zhang, J. Wang, *Sci. Robot.* **2017**, *2*, eaam6431.
- [22] W. Zhu, J. X. Li, Y. J. Leong, I. Rozen, X. Qu, R. F. Dong, Z. G. Wu, W. Gao, P. H. Chung, J. Wang, S. C. Chen, *Adv. Mater.* **2015**, *27*, 4411–4417.
- [23] H. Wang, J. G. S. Moo, M. Pumera, *ACS Nano* **2016**, *10*, 5041–5050.
- [24] J. Wang, *Lab Chip* **2012**, *12*, 1944–1950.
- [25] G. S. Huang, J. Y. Wang, Z. Q. Liu, D. K. Zhou, Z. A. Tian, B. R. Xu, L. Q. Li, Y. F. Mei, *Nanoscale* **2017**, *9*, 18590–18596.
- [26] J. Li, G. S. Huang, M. Ye, M. Li, R. Liu, Y. F. Mei, *Nanoscale* **2011**, *3*, 5083–5089.
- [27] J. Li, Z. Liu, G. S. Huang, Z. An, G. Chen, J. Zhang, M. Li, R. Liu, Y. F. Mei, *NPG Asia Mater.* **2014**, *6*, e94.
- [28] L. Li, J. Wang, T. Li, W. Song, G. Zhang, *Soft Matter* **2014**, *10*, 7511–7518.
- [29] M. Manjare, B. Yang, Y. P. Zhao, *J. Phys. Chem. C* **2013**, *117*, 4657–4665.
- [30] W. F. Paxton, S. Sundararajan, T. E. Mallouk, A. Sen, *Angew. Chem. Int. Ed.* **2006**, *45*, 5420–5429; *Angew. Chem.* **2006**, *118*, 5546–5556.
- [31] W. Gao, S. Sattayasamitsathit, J. Wang, *Chem. Rec.* **2012**, *12*, 224–231.
- [32] W. Gao, A. Uygun, J. Wang, *J. Am. Chem. Soc.* **2012**, *134*, 897–900.
- [33] A. A. Solovev, S. Sanchez, Y. F. Mei, O. G. Schmidt, *Phys. Chem. Chem. Phys.* **2011**, *13*, 10131–10135.
- [34] S. Sánchez, L. Soler, J. Katuri, *Angew. Chem. Int. Ed.* **2015**, *54*, 1414–1444; *Angew. Chem.* **2015**, *127*, 1432–1464.
- [35] T. L. Xu, W. Gao, L. P. Xu, X. J. Zhang, S. T. Wang, *Adv. Mater.* **2017**, *29*, 1603250.
- [36] J. X. Li, I. Rozen, J. Wang, *ACS Nano* **2016**, *10*, 5619–5634.
- [37] J. X. Li, W. Liu, J. Wang, I. Rozen, S. He, C. Chen, H. G. Kim, H. Lee, H. Lee, S. Kwon, T. Li, L. Li, J. Wang, Y. F. Mei, *Adv. Funct. Mater.* **2017**, *27*, 1700598.
- [38] M. Guix, C. C. Mayorga-Martinez, A. Merkoci, *Chem. Rev.* **2014**, *114*, 6285–6322.
- [39] F. Kuralay, S. Sattayasamitsathit, W. Gao, A. Uygun, A. Katzenberg, J. Wang, *J. Am. Chem. Soc.* **2012**, *134*, 15217–15220.
- [40] M. Ibele, T. E. Mallouk, A. Sen, *Angew. Chem. Int. Ed.* **2009**, *48*, 3308–3312; *Angew. Chem.* **2009**, *121*, 3358–3362.
- [41] A. A. Solovev, W. Xi, D. H. Gracias, S. M. Harazim, C. Deneke, S. Sanchez, O. G. Schmidt, *ACS Nano* **2012**, *6*, 1751–1756.
- [42] B. Jurado-Sánchez, J. Wang, A. Escarpa, *ACS Appl. Mater. Interfaces* **2016**, *8*, 19618–19625.
- [43] H. Wang, M. Pumera, *Chem. Rev.* **2015**, *115*, 8704–8735.
- [44] B. R. Xu, Y. F. Mei, *Sci. Bull.* **2017**, *62*, 525–527.
- [45] D. W. Yee, M. D. Schulz, R. H. Grubbs, J. R. Creer, *Adv. Mater.* **2017**, *29*, 1605293.
- [46] A. A. Pawar, S. Halivni, N. Waiskopf, Y. Ben-Shahar, M. SoreniHarari, S. Bergbreiter, U. Banin, S. Magdassi, *Nano Lett.* **2017**, *17*, 4497–4501.
- [47] I. Bernardeschi, O. Tricinci, V. Mattoli, C. Filippeschi, B. Mazzolai, L. Beccai, *ACS Appl. Mater. Interfaces* **2016**, *8*, 25019–25023.
- [48] M. G. Guney, G. K. Fedder, *J. Micromech. Microeng.* **2016**, *26*, 105011.
- [49] L. Folkertsma Hendriks, K. Zhang, M. A. Hempenius, G. J. Vancso, A. V. D. Berg, M. Odijk, *Polym. Adv. Technol.* **2017**, *28*, 1194–1197.
- [50] G. Gallino, F. Gallaire, E. Lauga, S. Michelin, *Adv. Funct. Mater.* **2018**, *28*, 1800686.
- [51] L. L. Wang, H. L. Zhu, Y. Shi, Y. Ge, X. M. Feng, R. Q. Liu, Y. Li, Y. W. Ma, L. H. Wang, *Nanoscale* **2018**, *10*, 11384–11391.
- [52] S. Hermanová, M. Pumera, *Nanoscale* **2018**, *10*, 7332–7342.
- [53] B. R. Zhang, G. S. Huang, L. Wang, T. B. Wang, L. Liu, Z. F. Di, X. Y. Liu, Y. F. Mei, *Chem. Asian J.* **2019**, DOI: 10.1002/asia.201900301.
- [54] J. Parmar, X. Ma, J. Katuri, J. Simmchen, M. M. Stanton, C. Trichet-Parades, L. Soler, S. Sanchez, *Sci. Technol. Adv. Mater.* **2015**, *16*, 014802.
- [55] V. V. Singh, K. Kaufmann, B. E. F. de ávila, E. Karshalev, J. Wang, *Adv. Funct. Mater.* **2016**, *26*, 6270–6278.
- [56] W. Gao, J. Wang, *Nanoscale* **2014**, *6*, 10486–10494.
- [57] T. Y. Huang, M. S. Sakar, A. Mao, A. J. Petruska, F. M. Qiu, X. B. Chen, S. Kennedy, D. Mooney, B. J. Nelson, *Adv. Mater.* **2015**, *27*, 6644–6650.

Manuscript received: February 28, 2019

Revised manuscript received: April 14, 2019

Accepted manuscript online: April 15, 2019

Version of record online: May 14, 2019